A model for seasonal changes in GPS positions and seismic wave speeds due to thermoelastic and hydrologic variations

Victor C. Tsai[1]

[1]   It is known that GPS time series contain a seasonal variation that is not due to tectonic motions, and it has recently been shown that crustal seismic velocities may also vary seasonally. In order to explain these changes, a number of hypotheses have been given, among which thermoelastic and hydrology-induced stresses and strains are leading candidates. Unfortunately, though, since a general framework does not exist for understanding such seasonal variations, it is currently not possible to quickly evaluate the plausibility of these hypotheses. To fill this gap in the literature, I generalize a two-dimensional thermoelastic strain model to provide an analytic solution for the displacements and wave speed changes due to either thermoelastic stresses or hydrologic loading, which consists of poroelastic stresses and purely elastic stresses. The thermoelastic model assumes a periodic surface temperature, and the hydrologic models similarly assume a periodic near-surface water load. Since all three models are two-dimensional and periodic, they are expected to only approximate any realistic scenario; but the models nonetheless provide a quantitative framework for estimating the effects of thermoelastic and hydrologic variations. Quantitative comparison between the models and observations is further complicated by the large uncertainty in some of the relevant parameters. Despite this uncertainty, though, I find that maximum realistic thermoelastic effects are unlikely to explain a large fraction of the observed annual variation in a typical GPS displacement time series or of the observed annual variations in seismic wave speeds in southern California. Hydrologic loading, on the other hand, may be able to explain a larger fraction of both the annual variations in displacements and seismic wave speeds. Neither model is likely to explain all of the seismic wave speed variations inferred from observations. However, more definitive conclusions cannot be made until the model parameters are better constrained.

1.   Introduction

[2]   Due to the importance of thermoelastic stresses and strains in engineered materials, the theory of thermoelasticity has a long and well developed history [see, e.g., *Love*, 1944; *Timoshenko and Goodier*, 1970]. Only in the past few decades, however, have thermoelastic effects been examined in a geologic context. In particular, *Berger* [1975] developed the theory to describe thermoelastic strains in a two-dimensional (2-D) homogeneous elastic half-space with a periodic surface temperature variation, and used this theory to describe how observed periodic strains within the Earth can be modeled satisfactorily. *Ben-Zion and Leary* [1986] expanded upon Berger's work to explicitly treat the same case but with an unconsolidated, incompetent surface layer above the elastic half-space. They found reasonable agreement between observed

strains at a few sites in southern California and strains modeled using observed temperature variations, with typical strains being on the order of 10^{-7}–10^{-6} and being delayed relative to the temperature variation by 2 to 3 months.

[3]   Hydrologic variability has also been studied for many years [e.g., *Todd*, 1959], primarily due to the importance of groundwater as a source of drinking water. However, the loading on the Earth produced by these variations has not been studied until more recently [e.g., *Crowley et al.*, 2006; *Bettinelli et al.*, 2008]. Fortunately, the theory that governs both the direct elastic loading and the poroelastic loading due to hydrologic variability is well understood. In fact, the theory of poroelasticity is known to have a one-to-one correspondence with the theory of thermoelasticity [*Biot*, 1956; *Rice and Cleary*, 1976].

[4]   GPS time series are well known to be affected by a potentially large number of factors, including tectonic motions, tidal loading, and the hydrologic cycle [*Dong et al.*, 2002]. *Prawirodirdjo et al.* [2006] further suggested that thermoelastic strains contribute significantly to the observed seasonal periodicity in GPS displacements (which has typical

[1]Geologic Hazards Science Center, U.S. Geological Survey, Golden, Colorado, USA.
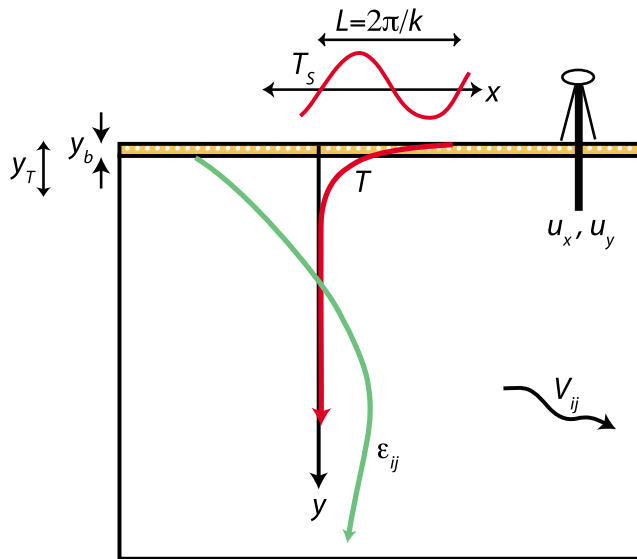
Figure 1. Schematic of the thermoelastic model. T_S is the surface temperature variation, y_T is the thermal boundary layer thickness, y_b is the thickness of the incompetent layer, and L is the wavelength of the surface temperature variation. The GPS station (with position u_x and u_y) is assumed anchored below y_T, and seismic velocities, V_{ij}, are calculated in the elastic half-space. Schematic depth profiles for temperature, $T(y)$, and strain, $\epsilon_{ij}(y)$, are graphed.

annual variations on the order of a few millimeters). *Prawirodirdjo et al.* [2006] found that the phase of the yearly variations in GPS positions could be well matched using the thermoelastic model of *Ben-Zion and Leary* [1986] with reasonable choices of parameters. However, in this study, the amplitudes of these variations were not considered, even though the displacements expected from thermoelastic strains are easily calculated by integrating the strains. In section 2.4, I provide expressions for these displacements and compare the calculated amplitudes with those observed (section 3.1). I find that estimates of the maximum realistic thermoelastic displacements can account for a fraction of the observed GPS signal at a typical site in southern California. *Bettinelli et al.* [2008] have also shown that direct elastic loading from water table variations can contribute to significant GPS displacements, and in section 2.4 I also calculate displacements corresponding with both this elastic effect and the poroelastic effect. I find that the maximum realistic hydrology-induced displacements can also account for a significant fraction of the observed GPS signal.

[5] Even more recently, by examining the coda of cross correlations of ambient seismic noise, *Meier et al.* [2010] have found a seasonal variation in observed seismic travel times in southern California. While there remains some possibility that these observations are due to seasonal variations in the location of seismic noise sources [e.g., *Zhan and Clayton*, 2010], the most straightforward interpretation of the observations is in terms of seasonal changes in seismic velocity structure on the order of $\delta V/V \approx 0.1\%$. *Meier et al.* [2010] suggest that two possible reasons for these temporal variations in seismic wave speed are hydrologic and/or thermoelastic variations, but do not estimate whether

the expected variability can produce the observed results. In section 2.5, I evaluate both of these hypotheses by calculating the expected wave speed variations using the third-order elasticity theory of *Murnaghan* [1951]. After performing order-of-magnitude estimates of certain parameters, I find that the calculated wave speed variations are unlikely to explain most of the observed variations (section 3.2), but that uncertainties in the parameters precludes making a stronger conclusion.

[6] Finally, before turning to the details, I would like to stress that the model results presented here, like many purely analytical results, can only be expected to approximate any given realistic scenario. Not only will it be seen that some of the model parameters are poorly constrained, but a number of approximations are also used that are not expected to hold perfectly. The usefulness of these analytical results are in understanding how quantitative results depend on the various key physical parameters, and in allowing researchers to quickly evaluate the plausibility of certain models explaining the observed phenomena. Since such plausibility studies have not yet been done to the extent performed here, I believe it to be useful for the community, as a step toward understanding the observations. I further believe that attempting more accurate and/or more precise quantitative analysis is not currently prudent, and should await further constraints.

## 2. Theoretical Results in Thermoelasticity and Poroelasticity

2.1. Berger's Thermoelastic Strain Solution

[7] *Berger* [1975] derived a solution to the uncoupled quasistatic thermoelastic equations [e.g., *Timoshenko and Goodier*, 1970; *Boley and Weiner*, 1997] for a 2-D elastic half-space in plane strain subjected to a sinusoidal surface temperature variation in both space and time. This 2-D approximation to a truly 3-D situation is used throughout this work; as in other periodic elasticity problems, 3-D effects are of second-order importance especially when wavelengths in one direction are considerably shorter than in the other direction [*Malvern*, 1969], and I do not attempt to include any of these dependencies. With x denoting horizontal position, y denoting depth, and t denoting time, the surface temperature boundary condition is given by

$$T(x, y = 0, t) - T_{avg} = T_0 \sin(kx) \cos(\omega t). \tag{1}$$

T_{avg} is a constant background average temperature, T_0 is half of the peak-to-peak amplitude of the periodic temperature variation, k is the horizontal wave number, and ω is frequency (see Figure 1). Assuming the temperature variation approaches zero at depth ($T(x, y \rightarrow \infty, t) - T_{avg} = 0$), Berger finds expressions for the strains ϵ_{xx}, ϵ_{yy} and ϵ_{xy}. These expressions contain "equivalent body force" terms that decay with depth in proportion to the temperature variation and "surface traction" terms that decay with depth proportional to e^{-ky}.

[8] For annual variations on the Earth ($\omega \approx 2 \cdot 10^{-7}$ s^{-1}) with kilometer-length scales and thermal diffusivity $\kappa \approx 10^{-6}$ m^2/s [*Berger*, 1975], then $\kappa k^2/\omega \ll 1$, and Berger finds that the expressions simplify significantly, especially for depths not within the thermal boundary layer. Using these approx-
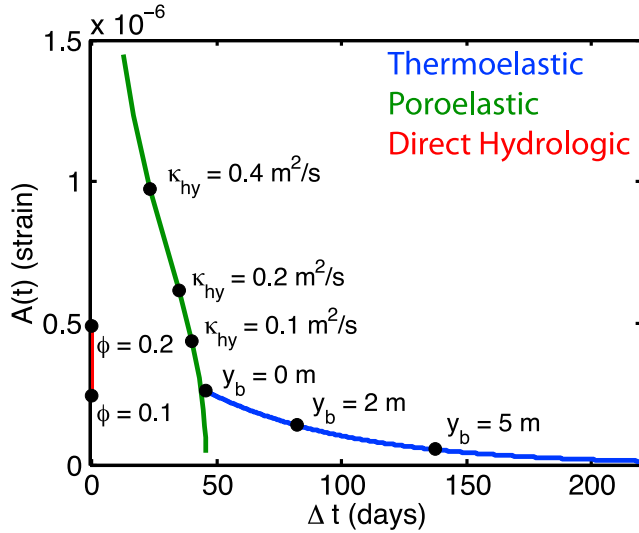
Figure 2. Strain amplitude $A(t)$ (amplitude only, without time dependence) as a function of time delay Δt. Thermoelastic results are for varying y_b, poroelastic results are for varying κ_{hy}, and water table elastic results are for varying ϕ. Maximum strain and minimum time delay for the thermoelastic solution occur when the incompetent layer thickness, y_b, is small. Maximum strain and minimum time delay for the poroelastic solution occur for the largest values of κ_{hy}. Maximum strain for the water table elastic solution occurs at the largest values of ϕ. Representative values of parameters are chosen as described in the text (e.g., $T_0 = 10°C$, $p_0 = 2.9 \cdot 10^4$ Pa). For Figure 2, $k = 2\pi/(10$ km$)$. Note that the thermoelastic and poroelastic amplitudes scale directly with k and that in section 3 it is suggested that k may actually be closer to $2\pi/(40$ km$)$.

imations and accounting for an incompetent layer of thickness y_b, as in the work of *Ben-Zion and Leary* [1986] (see Figure 1), I obtain simple expressions for the strains

$$\epsilon_{xx}(x,y,t) \approx A(t) \sin kx \cdot e^{-ky}[2(1 - \nu) - ky], \qquad (2a)$$

and

$$\epsilon_{yy}(x,y,t) \approx -A(t) \sin kx \cdot e^{-ky}[2\nu - ky], \qquad (2b)$$

and

$$\epsilon_{xy}(x,y,t) \approx A(t) \cos kx \cdot e^{-ky}[1 - ky], \qquad (2c)$$

where ν is Poisson's ratio and $A(t)$ is given by

$$A(t) = \frac{1+\nu}{1-\nu} k\alpha_{th} T_0 \sqrt{\frac{\kappa}{\omega}} e^{-\sqrt{\frac{\omega}{2\kappa}}y_b} \cos\left(\omega t - \sqrt{\frac{\omega}{2\kappa}}y_b - \frac{\pi}{4}\right). \quad (3)$$

In this expression, α_{th} is the coefficient of linear thermal expansion ($\alpha_{th} \approx 10^{-5}°C^{-1}$) [*Berger*, 1975], and equations (2) are appropriate for depths outside the thermal boundary layer, i.e., $y \gg \sqrt{\kappa/\omega}$. Examining equations (2), one observes that all components of the thermoelastic strain have

the same time dependence, similar amplitudes, and decay with depth in a similar fashion. Equation (3) shows that the strains are delayed relative to the temperature variation by an amount

$$\Delta t \equiv \frac{y_b}{\sqrt{2\omega\kappa}} + \frac{\pi}{4\omega} = \frac{y_b}{2}\sqrt{\frac{\tau}{\pi\kappa}} + \frac{\tau}{8}, \qquad (4)$$

where $\tau \equiv 2\pi/\omega$ is the period.

[9] Using equation (4) to solve for y_b in terms of Δt (and other parameters), we can rewrite $A(t)$ as a function of Δt as

$$A(t) = \frac{1+\nu}{1-\nu} k\alpha_{th} T_0 \sqrt{\frac{\kappa}{\omega}} e^{\pi/4 - \omega\Delta t} \cos[\omega(t - \Delta t)]. \qquad (5)$$

The strain amplitude versus phase lag of equation (5) is plotted in Figure 2 with $\nu = 0.3$, $k = 2\pi/(10$ km$)$, $T_0 = 10°C$, and other values as before ($\omega \approx 2 \cdot 10^{-7}$ s^{-1}, $\kappa \approx 10^{-6}$ m^2/s). The value of T_0 chosen is on the high end of representative temperature variations [*Berger*, 1975].

2.2. Poroelastic Hydrologic Modification

[10] Since thermoelasticity and poroelasticity share the same mathematical framework [*Biot*, 1956; *Rice and Cleary*, 1976; *Wang*, 2000], the corresponding decoupled quasistatic poroelastic problem is solved with the correspondence

$$\frac{\alpha_{th}ET}{1-2\nu} \leftrightarrow \alpha p, \qquad (6a)$$

$$\kappa \leftrightarrow \kappa_{hy}, \qquad (6b)$$

where E is Young's modulus, α is the Biot-Willis coefficient, p is pore pressure, and κ_{hy} is hydraulic diffusivity. For this problem, the boundary condition is

$$p(x, y = 0, t) - p_{avg} = p_0 \sin(kx) \cos(\omega t), \qquad (7)$$

where p_{avg} is a constant pressure and p_0 is the amplitude of the pore pressure variation. In reality, such a boundary condition does not exist but can be used to approximate variations in water table level. In addition, the decoupled approximation is not completely valid [*Detournay and Cheng*, 1993], but gives a reasonable approximation to the fully coupled problem [*Roeloffs*, 1988].

[11] For a nominal $\kappa_{hy} \approx 0.4$ m^2/s, $\hat{\kappa}_{hy} \equiv \kappa_{hy}k^2/\omega \approx 0.8$ does not satisfy $\hat{\kappa}_{hy} \ll 1$ as in the thermoelastic solution. However, the approximate solution is still roughly valid as long as $\hat{\kappa}_{hy} \lesssim 1$, with modification to equation (4) so that

$$\Delta t \equiv \frac{y_b}{\sqrt{2\omega\kappa_{hy}}} + \frac{\cot^{-1}\hat{\kappa}_{hy}}{2\omega} \approx \frac{\tau \cot^{-1}\hat{\kappa}_{hy}}{4\pi}, \qquad (8)$$

where the approximation is valid for $\kappa_{hy} \gtrsim 10^{-3}$ m^2/s (and $y_b < 10$ m). (Note that Berger's full unapproximated solution could be used if better precision were desired.) The approximate poroelastic solution is then given by equations (2) and (3) with equation (8) substituted for equation (4) and equations (6) replacing thermoelastic parameters. The strain amplitude versus phase lag is plotted in Figure 2 for a range of κ_{hy}, $E = 1.6 \cdot 10^{10}$ Pa, $p_0 = 2.9 \cdot 10^4$ Pa, $\alpha = 0.7$, and other values as

before. It is of interest to note that the strain amplitude and phase lag for the poroelastic solution for $\kappa_{hy} \approx 0.05$ m^2/s is nearly the same as that of the thermoelastic solution for $y_b = 0$.

2.3. Direct Elastic Hydrologic Modification

[12] In addition to the poroelastic effect just discussed, water table fluctuations also produce a direct elastic loading due to the weight of the additional fluid. This purely elastic loading can be calculated with the same methods as given by *Berger* [1975], yielding

$$\epsilon_{xx} = -A_e(t)\sin kx \cdot e^{-ky}[1 - 2\nu - ky], \qquad (9a)$$

$$\epsilon_{yy} = -A_e(t)\sin kx \cdot e^{-ky}[1 - 2\nu + ky], \qquad (9b)$$

$$\epsilon_{xy} = A_e(t)\cos kx \cdot e^{-ky} \cdot ky, \qquad (9c)$$

where $A_e(t)$ is given by

$$A_e(t) = \frac{(1+\nu)\phi p_0}{E}\cos(\omega t), \qquad (10)$$

and ϕ is porosity (so that fluid weight per unit area is ϕp). The primary difference between these strains and the poroelastic strains is that these strain amplitudes scale with $\phi p_0/E$ instead of $\alpha p_0\sqrt{\hat{\kappa}_{hy}}/E$ and the strains are exactly in phase with the water level forcing ($\Delta t = 0$). The strain amplitude for this direct elastic strain from water table fluctuations is plotted in Figure 2 for a range of ϕ, and other values as before. Note that for $\phi = 0.2$, the strain amplitude is similar to the poroelastic strain amplitude when $\kappa_{hy} = 0.15$ m^2/s.

2.4. GPS Displacements From Modeled Strain

[13] Given the strains of equations (2), it is straightforward to integrate to obtain displacements. By assumption, horizontal and vertical displacements, u_x and u_y, approach zero as $y \to \infty$ and rigid body motion is ignored. Therefore

$$u_y(x,y,t) = \int_\infty^y \epsilon_{y'y'}dy' \approx -\frac{A(t)}{k}\sin kx \cdot e^{-ky}[1 - 2\nu + ky], \qquad (11a)$$

and

$$u_x(x,y,t) = \int_{\pi/2k}^x \epsilon_{x'x'}dx' \approx -\frac{A(t)}{k}\cos kx \cdot e^{-ky}[2(1-\nu) - ky]. \qquad (11b)$$

[14] For a GPS station anchored at a point beneath the thermal boundary layer (see Figure 1), u_x and u_y of equations (11a) and (11b) are the temporal variations in GPS position expected of thermoelastic variations. GPS stations anchored within the thermal boundary layer (including at the surface) will include additional terms related to terms ignored in the approximations of equations (2). Under the approximations made, these additional terms are only significant for the vertical displacement, u_y. Integrating Berger's full solution, one finds that the magnitude of u_y would be increased by about a factor of 3 at the near surface if these terms were included. For the purposes of this paper, GPS stations will be assumed to be deeply anchored.

[15] For water table fluctuations, the same analysis applies. Equations (11a) and (11b) apply to poroelastic displacements with the modifications of equations (6) and (8), and equations (9) can similarly be integrated to obtain displacements for the purely elastic component. However, since actual water table fluctuations occur at depths of a few meters and furthermore $\kappa_{hy} \gg \kappa$, the GPS stations are likely anchored within the "porous" boundary layer. Thus, there are additional poroelastic displacements as discussed in the previous paragraph. Since only the vertical displacement, u_y, is significantly affected and only horizontal displacements are compared, these additional displacements will not be discussed further.

2.5. Seismic Wave Speed Variation From Modeled Strain

[16] For a given strain field, expressions for elastic wave speeds can be obtained by keeping up to third-order terms in the strain energy function [*Murnaghan*, 1951; *Norris*, 1998]. For an initially isotropic body, *Hughes and Kelly* [1953] and *Egle and Bray* [1976] provide V_{11}, V_{12} and V_{13} as

$$\rho_0 V_{11}^2 = \lambda + 2\mu + (2l + \lambda)\theta + (4m + 4\lambda + 10\mu)\epsilon_1, \qquad (12a)$$

$$\rho_0 V_{12}^2 = \mu + (\lambda + m)\theta + 4\mu\epsilon_1 + 2\mu\epsilon_2 - n\epsilon_3/2, \qquad (12b)$$

and

$$\rho_0 V_{13}^2 = \mu + (\lambda + m)\theta + 4\mu\epsilon_1 + 2\mu\epsilon_3 - n\epsilon_2/2, \qquad (12c)$$

where V_{ij} is the speed propagating in the i direction with polarization in the j direction, ρ_0 is the initial density, λ and μ are the Lame constants ($\lambda = E\nu/[(1+\nu)(1-2\nu)]$, $\mu = E/[2(1+\nu)]$, where E is Young's modulus), ϵ_i are the principal strains, $\theta = \epsilon_1 + \epsilon_2 + \epsilon_3$, and l, m and n are the Murnaghan third-order elastic constants.

[17] Rotating equations (2) into principal strain coordinates, then

$$\epsilon_{1,2} = A(t)e^{-ky}[\sin kx \cdot (1 - 2\nu) \pm (1 - ky)], \qquad (13)$$

and $\epsilon_3 = 0$ (plane strain). (The $\pm$ is $+$ for the first subscript, $-$ for the second subscript.) In this coordinate system, thermoelastic and poroelastic relative wave speed changes can be expressed as

$$\frac{\Delta V_{11,22}}{V_{11,22}^0} \approx \frac{A(t)e^{-ky}}{\lambda + 2\mu}[\pm(2\lambda + 5\mu + 2m)(1 - ky) + (3\lambda + 5\mu + 2l + 2m)\sin kx(1 - 2\nu)], \qquad (14a)$$

$$\frac{\Delta V_{12,21}}{V_{12,21}^0} \approx A(t)e^{-ky}\left[\pm(1 - ky) + \frac{\lambda + 3\mu + m}{\mu}\sin kx(1 - 2\nu)\right], \qquad (14b)$$

and

$$\frac{\Delta V_{13,23}}{V_{13,23}^0} \approx A(t)e^{-ky}\left[\pm(2 + n/4\mu)(1 - ky) + \frac{\lambda + 2\mu + m - n/4}{\mu}\sin kx(1 - 2\nu)\right], \qquad (14c)$$

where V_{ij}^0 are the wave speeds in the unstressed body, and the expressions are accurate for small $\Delta V/V^0$. Using the elastic strains of equation (9) results in identical expressions except with $A_e(t)$ replacing $A(t)$ and ky replacing $(1 - ky)$.

[18] Equation (14a) expresses the P wave component of the relative change in elastic wave speeds, whereas equations (14b) and (14c) express the S-wave components. Since the 1–2 axes do not (in general) line up with the $x - y$ axes, only quasi-P, quasi-SV and quasi-SH waves exist in the $x - y - z$ coordinate system. For the same reason, only quasi-Rayleigh and quasi-Love waves exist, and there remains coupling between them [e.g., *Anderson*, 1961]. However, approximate expressions for these anisotropic Rayleigh and Love wave components can be computed [*Backus*, 1970; *Smith and Dahlen*, 1973; *Crampin*, 1981]. It may be of use to note, also, that the anisotropic expressions of equations (14a), (14b), and (14c) share an isotropic component (terms multiplying $\sin kx$) in addition to the anisotropic component (terms multiplying $1 - ky$), so that there exists an isotropic part to the thermoelastic wave speed variations. Finally, one should note that all expressions make use of "average" Murnaghan constants that are assumed to be uniform throughout the entire half-space, an assumption that may not be very realistic.

3. Comparison of Seasonal Observations With Modeled Annual Variations

[19] In the following subsections, I use the theory presented in section 2 to estimate whether it is possible for the three models discussed (thermoelastic, poroelastic hydrologic, and direct elastic hydrologic response) to explain the displacements and wave speed variations observed in southern California. The general approach taken is to use estimates of model parameters that are realistic but generous in terms of producing the desired effect, and to compare these "maximum realistic" model results with single observations that are representative of the southern California region. For example, as model parameters I choose temperature and water table amplitudes that are among the highest observed in southern California. The reasoning behind such a choice is that if these maximum realistic models are still unable to produce the desired effect, these models can be falsified more convincingly as being large contributors to the observed effect. It should be noted that the ability of some of these maximum realistic models to reach observed levels only implies that those models are potentially credible, not that they necessarily explain the observations everywhere throughout southern California (or elsewhere). Finally, as described in more detail below, model uncertainties are significantly higher for seismic wave speed variations than for displacements; nonetheless, as will be shown, all of the models require parameter choices outside the likely realistic range in order to produce wave speed variations that are in the observational range.

3.1. GPS Observations

[20] GPS displacement time series are well known to have seasonal variability [*Dong et al.*, 2002] and a subsequent study by *Prawirodirdjo et al.* [2006] suggested that thermoelastic strains are a significant contributor to this variability. However, despite successfully matching much of the observed signal, *Prawirodirdjo et al.* [2006] do not attempt to quantitatively compare the observations with the thermoelastic model. In particular, they compare horizontal GPS displacements with calculated horizontal strains by arbitrarily scaling the amplitudes, without attempting to account for the fact that local displacements could have been determined from the modeled strain field. Comparison of equation (2a) with equation (11b) shows that u_x has a spatial variability exactly out of phase with ϵ_{xx}. Furthermore, once k and Δt are determined, the amplitudes of the thermoelastic displacements are no longer arbitrary and can be calculated using equations (11a) and (11b). To make a quantitative comparison of the models with the observations, I apply the results of section 2.4 to the observations of *Prawirodirdjo et al.* [2006]. It should be noted that the direct elastic displacements from water table variability have been modeled previously by *Bettinelli et al.* [2008], and that *Bawden et al.* [2001] and *Watson et al.* [2002] have previously suggested groundwater seasonality to be important.

3.1.1. Thermoelastic Model Comparison

[21] In using equation (11b) to calculate the annual variability in horizontal displacements, I choose representative values of parameters as before. To summarize, I take $\nu = 0.3$, $\alpha_{th} = 10^{-5}°C^{-1}$, $\kappa = 10^{-6}$ m^2/s, $\omega = 2 \cdot 10^{-7}$ s^{-1}. To approximately match the data of *Prawirodirdjo et al.* [2006], I further take $T_0 = 10°C$, $k = 2\pi/(20$ km$)$, $y_b = 0.5$ m. The value of T_0 is chosen to match the high end of observed temperature variations in southern California (specifically, matching the annual Fourier component of the temperature record from Palm Springs as shown in Figure 3a); the value of k is chosen to fit the spatial variability in the observations; and the value of y_b is chosen to fit the phase delay of the thermoelastic variations relative to the observed temperature variations, as described in equation (4). Here, and below, best-estimate values are provided.

[22] The horizontal displacement, u_x, is evaluated at $y \approx 0$ (close to the surface, where the GPS station is assumed to be anchored). Substituting these numbers into equation (11b) results in

$$u_x(x, 0, t) \approx -0.5 \text{ mm} \cdot \cos kx \cdot \cos[2\pi(t - 55 \text{ days})/\tau]. \quad (15)$$

The observed amplitudes of GPS annual variability in the study region are about 2 mm. Thus, the thermoelastic displacements calculated could potentially represent a significant fraction ($\approx 25\%$) of the observed displacements (see Figure 3b). Some of the parameter values (e.g., thermal diffusivity or thermal expansion coefficient) have some uncertainty and heterogeneity, and a slightly higher fraction of the observed signal could potentially be explained with appropriate modification of those values. One may note that after substitution of equation (5), equation (11b) is independent of k, has an amplitude that decays exponentially with y_b, and is proportional to T_0. It is likely that some fraction of the temperature fluctuation is recorded uniformly by the subsurface (resulting in a uniform temperature field without thermoelastic strains), implying a lower value of T_0 and therefore explaining a smaller fraction of the observed displacements. Moreover, as stated above, the value of T_0 used is already on the high end of observed values. It is therefore likely that the thermoelastic model achieves less than 25% of the observed displacement amplitude.
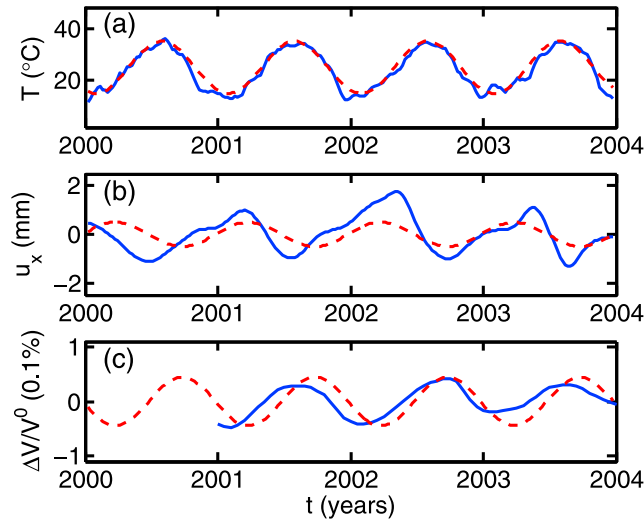
Figure 3. Comparison of observed (solid blue) and modeled (dashed red) (a) T, (b) u_x, and (c) $\Delta V/V^0$ as a function of time. All model results are shown at the horizontal position, x, for which the signal is largest. (Figure 3a) Smoothed temperature record from Palm Springs Airport (PSP) and modeled temperature with $T_0 = 10°C$. (Figure 3b) Approximate averaged GPS N-S ground displacement from the 29 Palms region of *Prawirodirdjo et al.* [2006] and the modeled displacement of equation (15). The chosen GPS record is representative of displacements observed in the region; details regarding the GPS observation and site conditions are given by *Prawirodirdjo et al.* [2006]. (Figure 3c) Approximate averaged $\Delta V/V^0$ observed by *Meier et al.* [2010] in the Los Angeles basin and the modeled $\Delta V_{SV}/V_{SV}^0$ of equation (18) with $m/\mu = 10^4$.

[23] The spatial dependence of u_x on $-\cos kx$ given a temperature variation with dependence on $\sin kx$ suggests that if thermoelastic variations are a significant component of the observed displacements then the maximum subsurface temperature variations occur spatially out of phase with the maximum observed displacements. This conclusion is counter to that assumed by *Prawirodirdjo et al.* [2006].

3.1.2. Hydrologic Model Comparisons

[24] For variations in water table level, I use equation (11b) to calculate the poroelastic horizontal displacement and the equivalently integrated form of equation (9a) to calculate the direct elastic horizontal displacement. As before, for parameter values I use $E = 1.6 \cdot 10^{10}$ Pa, $\alpha = 0.7$ and $\phi = 0.15$ to approximate sandstone values from *Detournay and Cheng* [1993]; and I use $p_0 = 2.9 \cdot 10^4$ Pa, equivalent to height of water of $h_0 = 3$ m, to match observed water table variation in the (Los Angeles) region (see Figure 4a). Values of κ_{hy} for sandstone vary substantially, from 0.005 m^2/s to 1.6 m^2/s [*Detournay and Cheng*, 1993]; here, I use 0.4 m^2/s as a nominal value, but note that this could be significantly different from the true value. I also note that the value of p_0 (or equivalently, h_0) also varies spatially in a significant manner; for example, some parts of southern California, such as the Mojave region, receive less rain than the Los Angeles region and have smaller values of p_0 and h_0.

[25] Evaluating the modeled u_x as previously, I obtain the results as plotted in Figures 4b and 4d for the poroelastic

and direct elastic effects, respectively. As shown, both of these models have order-of-magnitude agreement with the amplitude of the observations, with a slight overprediction (by about 10%–30%). The phase of both models is reasonable but does not match the observations perfectly, partly due to the fact that the observations have subyearly Fourier components whereas the models have a single prescribed annual component. It should be noted that some of the overprediction is likely due to using a value of p_0 larger than is appropriate for the 29 Palms region where the GPS observations are taken; some of the overprediction may also be due to the fact that the direct elastic and poroelastic effects tend to cancel each other (they would have exactly opposite signs for large values of κ_{hy}), with the true effect being equivalent to the difference in the two signals. Finally, the overprediction may also be because the 29 Palms observations are not entirely representative of displacements in the southern California region; for example, for a similar region, *Watson et al.* [2002] find peak-to-peak displacements on the order of 6 mm, rather than the 4 mm of *Prawirodirdjo et al.* [2006].
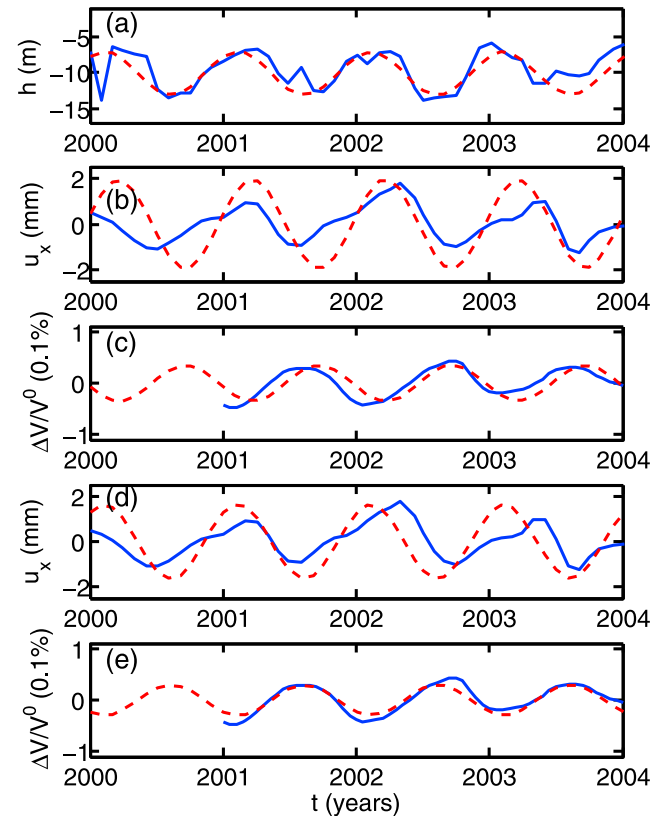
Figure 4. Comparison of observed (solid blue) and modeled (dashed red) quantities from water table variability. (a) Water table record from California state well 04S12W36J001S in Rossmoor, California (http://www. water.ca.gov) and modeled water table with $h_0 = 3$ m, corresponding to $p_0 = 2.9 \cdot 10^4$ Pa. (b and c) Comparisons equivalent to those in Figures 3b and 3c but for poroelastic effects. (d and e) Comparisons equivalent to those in Figures 3b and 3c but for direct elastic effects. Both Figures 4c and 4e use the less extreme choice of $m/\mu = 2 \cdot 10^3$.

3.1.3. Summary of GPS Displacement Comparison

[26] Based on the above considerations, I conclude that thermoelastic variations may be responsible for an observable fraction of the annual variability of horizontal GPS displacements but that it is not likely to explain the entire annual signal even in places with large temperature fluctuations. I further conclude that in regions with significant water table variability, those variations could potentially explain the full signal through either the direct elastic effect, the poroelastic effect, or a combination. The sum of the three contributions could also potentially explain the observations better than any single model (especially with regards to the precise phasing of the signal, which is not well fit by any of the models alone). Given the difficulties of knowing precise values of some parameters such as the hydraulic diffusivity and thermal expansion coefficient, there remains some ambiguity in these conclusions. However, given that the calculations shown represent "maximum realistic" models, I believe it prudent to consider alternative mechanisms for causing the remainder of the observed seasonal signal. *Dong et al.* [2002] and *Hill et al.* [2009] list some potential alternatives that include atmospheric effects and other environmental influences.

3.2. Seismic Observations

[27] The recent study of *Meier et al.* [2010] found seasonal variations in the travel time of seismic coda that they interpret to be due to changes in wave speed. The authors further suggest that these changes in wave speed may be due to thermoelastic or hydrologic effects, but do not attempt to evaluate their hypotheses. Previous studies [*Whitcomb et al.*, 1973; *Clymer and McEvilly*, 1981; *Li et al.*, 2007] have also suggested that hydrologic changes are important. In order to test the plausibility of these claims, I use the results of section 2.5 to calculate (the magnitude and phase of) the change in wave speeds expected of annual thermoelastic and hydrologic variations. In order to make this comparison, though, a number of complications remain. First of all, Murnaghan's third-order elastic constants (l, m and n) are poorly constrained for the geologic materials of interest. Much of the work done on geologic materials has focused on the changes in elastic constants due to changes in uniform pressure [e.g., *Lee et al.*, 2004; *Gret et al.*, 2006; *Larose and Hall*, 2009], with a smaller number of materials (e.g., pyrex, iron, steel, sandstone, shale and concrete) having complete characterization of the 3 Murnaghan constants [*Hughes and Kelly*, 1953; *Egle and Bray*, 1976; *Johnson and Rasolofosaon*, 1996; *Sarkar et al.*, 2003; *Prioul et al.*, 2004; *D'Angelo et al.*, 2008; *Payan et al.*, 2009], and none of these experiments being done at high pressures or temperatures. Given the large variability in the values of the Murnaghan constants, with l, m and n all varying in the range $\pm 10^{14}$ Pa (i.e., of magnitudes up to 1000 times larger than the Lame constants, and not necessarily of one sign), I believe it premature to attempt a truly quantitative comparison of observations with theory. Instead, I estimate roughly how large the Murnaghan constants must be in order to achieve reasonable fits to the observations, and compare these estimates with the range of measured values. While such a comparison may be unsatisfying, my opinion is that such constraints are better than a complete lack of quantitative constraints.

[28] *Johnson and Rasolofosaon* [1996], *D'Angelo et al.* [2008] and *Payan et al.* [2009] suggest that the Murnaghan constants in rock are typically negative and 2 to 4 orders of magnitude larger than the Lame constants. While these experiments are not done at appropriate confining stresses to truly be applicable to the depths discussed here, they represent the best constraints currently in the literature. Thus, as a first estimate, I take the Murnaghan constants (l, m and n) to range between -100 and $-10,000$ times the Lame constants (λ and μ). Equations (14a), (14b), and (14c) can then all be written as $A(t)e^{-ky}(C_1 + C_2 ky)$, with nondimensional constants C_1 and C_2 in the range $\pm 10^{2-5}$. One can therefore roughly estimate an upper bound on $\Delta V/V^0$ to be

$$\left| \frac{\Delta V}{V^0} \right| \lesssim 10^5 |A(t)| e^{-ky}(1 + ky). \tag{16}$$

More importantly, under these same approximations, all in-plane V_S variations are given by

$$\frac{\Delta V_{12,21}}{V^0_{12,21}} \approx \frac{m}{\mu} A(t) e^{-ky} \sin kx (1 - 2\nu), \tag{17}$$

so that they are approximately isotropic and only depend on Murnaghan constant m. This is of interest because the observed $\Delta V/V^0$ are for Rayleigh waves, which are primarily sensitive to $V_{SV} \equiv V_{xy} = V_{12} = V_{21}$. One may also note that the direct elastic version of equation (17) is identical except with $A_e(t)$ replacing $A(t)$.

3.2.1. Thermoelastic Model Comparison

[29] Taking representative values as in section 3.1.1, I obtain

$$\frac{\Delta V_{SV}}{V^0_{SV}} \approx 4 \cdot 10^{-8} \frac{m}{\mu} \cos[2\pi(t - 55 \text{ days})/\tau] e^{-ky} \sin kx \tag{18}$$

Compared to the observed $\Delta V/V^0 \approx (0.2 - 1) \cdot 10^{-3}$ [*Meier et al.*, 2010], the calculated thermoelastic changes in wave speed are plausibly in the right amplitude range if m/μ is close to the maximum possible value of $\approx -10,000$, which would give a wave speed perturbation of amplitude $0.4 \cdot 10^{-3}$ (see Figure 3c). One may note that it is perhaps unlikely that these extreme values are reached for average sandstones, for which m/μ are typically in the range -200 to -1000 [*D'Angelo et al.*, 2008], with the most extreme values occurring for highly cracked specimens [*Johnson and Rasolofosaon*, 1996]. (Under the large confining stresses appropriate for the $\approx$ few kilometer depths considered, seismic wave speeds in the highly cracked specimens should be less sensitive to applied stresses and therefore have smaller magnitude Murnaghan constants.)

[30] Equation (18) also shows that these changes in velocity exponentially decrease with depth with a length scale of $1/k \approx 3.2$ km (using the k from section 3.1). Since the observed $\Delta V/V^0$ are for Rayleigh-wave coda in the period range 0.5–10 s [*Meier et al.*, 2010], which generally have sensitivity to depths of $\approx$1–20 km, the short-period range of the observations is expected to sample primarily near-surface $V_{SV} \equiv V_{xy}$ (i.e., vertically polarized shear waves in the range $ky \ll 1$); on the other hand, the long-period range will have diminished amplitudes due to the Rayleigh wave kernel having sensitivity to depths outside the thermoelastic expo-

nential tail. The observations of *Meier et al.* [2010] do not clearly display this dependence of perturbation amplitude on period, and in fact may show the opposite trend, but the difference may not be resolved. Furthermore, it should be noted that *Meier et al.* [2010] observe the wave speed variations even when averaged over the entire Los Angeles basin, which has a horizontal length scale of roughly 40 km. The spatial wavelength of 20 km (and associated k) that is used to match the data of *Prawirodirdjo et al.* [2006] therefore cannot explain this aspect of the seismic observations. Arbitrarily choosing a spatial wavelength of 80 km instead, however, does not improve comparisons because it results in a fourfold decrease in k, and therefore a fourfold decrease in $A(t)$ and $\Delta V/V^0$.

[31] The phase of the calculated thermoelastic signal may also be somewhat different from the observed seismic wave speed variations. The temperature variations peak approximately in February and August of each year. This results in a thermoelastic variation peak as early as late March and late September, but potentially up to 2 months later, depending on exactly how thick the incompetent layer (y_b) is (see Figure 2). However, the observations of *Meier et al.* [2010] seem to peak roughly in January–February and September–October (with some variability). Thus, while the autumn peak may have approximately the right phase to be explained through thermoelastic variations, the winter/spring peak is offset (too early) by a significant amount (a minimum of about 1 month) (see Figure 3c). Interestingly, this uneven variation (with a faster wave speed decrease and a slower wave speed increase) is qualitatively similar to the uneven variation in observed strains and GPS displacements [*Ben-Zion and Leary*, 1986; *Prawirodirdjo et al.*, 2006], though neither of these features are well modeled with purely thermoelastic effects. This also suggests that phenomena other than thermoelasticity may be important for explaining the observations. As proposed by *Meier et al.* [2010], one possibility for this unexplained offset in phase is that seasonal hydrologic changes simply affect the thermoelastic parameters enough, e.g., through the known dependence of l, m and n on water content [*Johnson and Rasolofosaon*, 1996]. This may explain why the observed wave speed variation is more robust within the Los Angeles basin [*Meier et al.*, 2010]; otherwise, the thermoelastic model has difficulty explaining this fact. In the following section, I only assess how well the pure hydrologic effect explains the observations.

3.2.2. Hydrologic Model Comparisons

[32] Taking representative values as in section 3.1.2, keeping k as before (so as to obtain a similar comparison), and using the poroelastic modifications of equations (6), I obtain

$$\frac{\Delta V_{SV}}{V_{SV}^0} \approx 17 \cdot 10^{-8} \frac{m}{\mu} \cos[2\pi(t - 35 \text{ days})/\tau] e^{-ky} \sin kx \quad (19)$$

for the poroelastic effect. For the direct elastic effect, using the elastic modification to equation (17) gives

$$\frac{\Delta V_{SV}}{V_{SV}^0} \approx 14 \cdot 10^{-8} \frac{m}{\mu} \cos[2\pi(t - 0 \text{ days})/\tau] e^{-ky} \sin kx. \quad (20)$$

Again comparing with *Meier et al.* [2010], I find that both the poroelastic effect and the direct elastic effect from water

table variability produce changes in wave speed that are plausibly in the right amplitude range if $m/\mu \approx -2 \cdot 10^3$ (see Figures 4c and 4e). Compared to the value needed for the thermoelastic calculation (-10^4), this is closer to the likely range of m/μ, though still on the high end compared to the average sandstone values of -200 to -1000 [*D'Angelo et al.*, 2008].

[33] As with the thermoelastic model, the value of k used in these calculations is likely at least a factor of 4 too large for two reasons. For one, the observed wave speed variations occur fairly deep (deeper than the exponential tail with the given k would suggest) and, second, the wave speed variations seem to be consistent across a 40 km horizontal length scale. Interestingly, although the poroelastic $A(t)$ is directly proportional to k, $A_e(t)$ contains no k dependence. Therefore, decreasing k (by a factor of 4) results in a smaller $\Delta V/V^0$ (by a factor of 4) for the poroelastic effect but does not affect the direct elastic effect. This suggests that the direct elastic response from water table variations is most likely to best explain the observed wave speed variations. Comparing the phase of the modeled signals with the observations of *Meier et al.* [2010] (see Figure 4), I also observe that the direct elastic response does a slightly better job with the phase. However, as discussed for the GPS displacements, the existence of subyearly Fourier components in the observations makes it difficult to be certain of which (single frequency) model agrees better with the observed phasing.

3.2.3. Summary of Seismic Wave Speed Comparison

[34] Based on the above considerations, I conclude that thermoelastic variations are unlikely to explain the observed annual variability in seismic wave speeds. Hydrologic variations, on the other hand, potentially better explain the observations, with the direct elastic effect having a stronger, more robust signal compared to the poroelastic effect. However, even the direct elastic effect requires m/μ to be on the very high end of what may be expected. This questionable agreement suggests that it is prudent to consider alternative hypotheses regarding both the likely models for causing seasonal velocity changes as well as the interpretation of the observations as seismic velocity changes [e.g., *Zhan and Clayton*, 2010]. I emphasize, though, that due to the uncertainties in many important parameters, including order-of-magnitude uncertainty in the Murnaghan constants, there remains some ambiguity in these conclusions.

4. Conclusions

[35] I present simple expressions for the GPS displacements and wave speed variations expected of thermoelastic and hydrology-induced annual variations. The thermoelastic model assumes a periodic surface temperature field whereas the hydrologic model assumes periodic fluctuations in water table levels. I then use these expressions to compare calculations of annual variations with observations of GPS variations [*Prawirodirdjo et al.*, 2006] and wave speed variations [*Meier et al.*, 2010]. For GPS, I find that thermoelastic displacements can explain a significant fraction of the observed annual variations (perhaps up to 25%), but likely not the entire signal. Hydrology-induced (poroelastic and direct elastic) displacements can explain the full amplitude of the observed annual variations, and may even overpredict the

amplitudes. Phases for all three models can be partially matched with appropriate choice of free parameters.

[36] For seismic wave speeds, I find that thermoelastic variations can only explain the observed variations with extremely high values of the Murnaghan constants (which are unlikely to exist); similarly, hydrology-induced variations also require very high values for these constants to explain the observations, though not as extreme. Of the three models, the direct elastic effect from hydrologic loading is able to explain the observations the best but still requires values of the Murnaghan constants that may not be realistic. This questionable agreement suggests that alternative hypotheses be considered either for models or for interpretations of the observations. However, I emphasize that the Murnaghan constants for relevant materials must be much better characterized if a truly accurate quantitative comparison is to be made. Phases can also only be partially matched, possibly suggesting that other seasonal processes may be important, but perhaps only that subyearly Fourier components must be included in the analysis. Due to a large amount of uncertainty and potential heterogeneity in many model parameters, none of the conclusions drawn here should be taken as definitive; more precise constraints must await better measurements of the relevant parameters.

References

Anderson, D. L. (1961), Elastic wave propagation in layered anisotropic media, *J. Geophys. Res.*, 66, 2953–2963.

Backus, G. (1970), A geometrical picture of anisotropic elastic tensors, *Rev. Geophys. Space Phys.*, 8, 633–671.

Bawden, G. W., W. Thatcher, R. S. Stein, K. W. Hudnut, and G. Peltzer (2001), Tectonic contraction across Los Angeles after removal of groundwater pumping effects, *Nature*, 412, 812–815.

Ben-Zion, Y., and P. Leary (1986), Thermoelastic strain in a half-space covered by unconsolidated material, *Bull. Seismol. Soc. Am.*, 76, 1447–1460.

Berger, J. (1975), A note on thermoelastic strains and tilts, *J. Geophys. Res.*, 80, 274–277.

Bettinelli, P., J.-P. Avouac, M. Flouzat, L. Bollinger, G. Ramillien, S. Rajaure, and S. Sapkota (2008), Seasonal variations of seismicity and geodetic strain in the Himalaya induced by surface hydrology, *Earth Planet. Sci. Lett.*, 266, 332–344.

Biot, M. A. (1956), Thermoelasticity and irreversible thermodynamics, *J. Appl. Phys.*, 27, 240–253.

Boley, B. A., and J. H. Weiner (1997), *Theory of Thermal Stresses*, Dover, New York.

Clymer, R. W., and T. V. McEvilly (1981), Travel-time monitoring with vibroseis, *Bull. Seismol. Soc. Am.*, 71, 1903–1927.

Crampin, S. (1981), A review of wave motion in anisotropic and cracked elastic-media, *Wave Motion*, 3, 343–391.

Crowley, J. W., J. X. Mitrovica, R. C. Bailey, M. E. Tamisiea, and J. L. Davis (2006), Land water storage within the Congo Basin inferred from GRACE satellite gravity data, *Geophys. Res. Lett.*, 33, L19402, doi:10.1029/2006GL027070.

D'Angelo, R. M., K. W. Winkler, and D. L. Johnson (2008), Three wave mixing test of hyperelasticity in highly nonlinear solids: Sedimentary rocks, *J. Acoust. Soc. Am.*, 123, 622–639.

Detournay, E., and A. H.-D. Cheng (1993), Fundamentals of poroelasticity, in *Comprehensive Rock Engineering: Principles, Practice and Projects*, vol. 2, edited by J. A. Hudson, Pergamon Press, Oxford, U. K.

Dong, D., P. Fang, Y. Bock, M. K. Cheng, and S. Miyazaki (2002), Anatomy of apparent seasonal variations from GPS-derived site position time series, *J. Geophys. Res.*, 107(B4), 2075, doi:10.1029/2001JB000573.

Egle, D. M., and D. E. Bray (1976), Measurement of acoustoelastic and third-order elastic constants for rail steel, *J. Acoust. Soc. Am.*, 60, 741–744.

Gret, A., R. Snieder, and J. Scales (2006), Time-lapse monitoring of rock properties with coda wave interferometry, *J. Geophys. Res.*, 111, B03305, doi:10.1029/2004JB003354.

Hill, E. M., J. L. Davis, P. Elosegui, B. P. Wernicke, E. Malikowski, and N. A. Niemi (2009), Characterization of site-specific GPS errors using a short-baseline network of braced monuments at Yucca Mountain, southern Nevada, *J. Geophys. Res.*, 114, B11402, doi:10.1029/2008JB006027.

Hughes, D. S., and J. L. Kelly (1953), Second-order elastic deformation of solids, *Phys. Rev.*, 92, 1145–1149.

Johnson, P. A., and P. N. J. Rasolofosaon (1996), Nonlinear elasticity and stress-induced anisotropy in rock, *J. Geophys. Res.*, 101, 3113–3124.

Larose, E., and S. Hall (2009), Monitoring stress related velocity variation in concrete with a 2 × 10-5 relative resolution using diffuse ultrasound, *J. Acoust. Soc. Am.*, 125, 1853–1856.

Lee, K. K. M., B. O'Neill, W. R. Panero, S.-H. Shim, L. R. Benedetti, and R. Jeanloz (2004), Equations of state of the high-pressure phases of a natural peridotite and implications for the Earth's lower mantle, *Earth Planet. Sci. Lett.*, 223, 381–393.

Li, Y.-G., P. Chen, E. S. Cochran, and J. E. Vidale (2007), Seismic velocity variations on the San Andreas fault caused by the 2004 M6 Parkfield Earthquake and their implications, *Earth Planets Space*, 59, 21–31.

Love, A. E. H. (1944), *A Treatise on the Mathematical Theory of Elasticity*, 4th ed., Dover, New York.

Malvern, L. E. (1969), *Introduction to the Mechanics of a Continuous Medium*, Prentice-Hall, Upper Saddle River, N. J.

Meier, U., N. M. Shapiro, and F. Brenguier (2010), Detecting seasonal variations in seismic velocities within Los Angeles basin from correlations of ambient seismic noise, *Geophys. J. Int.*, 181, 985–996, doi:10.1111/j.1365-246X.2010.04550.x.

Murnaghan, F. D. (1951), *Finite Deformation of an Elastic Solid*, Wiley, New York.

Norris, A. N. (1998), Finite-amplitude waves in solids, in *Nonlinear Acoustics*, edited by M. F. Hamilton and D. T. Blackstock, Academic Press, New York.

Payan, C., V. Garnier, J. Moysan, and P. A. Johnson (2009), Determination of third order elastic constants in a complex solid applying coda wave interferometry, *Appl. Phys. Lett.*, 94, 1–3.

Prawirodirdjo, L., Y. Ben-Zion, and Y. Bock (2006), Observation and modeling of thermoelastic strain in southern California Integrated GPS Network daily position time series, *J. Geophys. Res.*, 111, B02408, doi:10.1029/2005JB003716.

Prioul, R., A. Bakulin, and V. Bakulin (2004), Nonlinear rock physics model for estimation of 3D subsurface stress in anisotropic formations: Theory and laboratory verification, *Geophysics*, 69, 415–425.

Rice, J. R., and M. P. Cleary (1976), Some basic stress diffusion solutions for fluid-saturated elastic porous media with compressible constituents, *Rev. Geophys. Space Phys.*, 14, 227–241.

Roeloffs, E. A. (1988), Fault stability changes induced beneath a reservoir with cyclic variations in water level, *J. Geophys. Res.*, 93, 2107–2124.

Sarkar, D., A. Bakulin, and R. L. Kranz (2003), Anisotropic inversion of seismic data for stressed media: Theory and a physical modeling study on Berea Sandstone, *Geophysics*, 68, 690–704.

Smith, M. L., and F. A. Dahlen (1973), The azimuthal dependence of Love and Rayleigh wave propagation in a slightly anisotropic medium, *J. Geophys. Res.*, 78, 3321–3333.

Timoshenko, S. P., and J. N. Goodier (1970), *Theory of Elasticity*, 3rd ed., McGraw-Hill, Singapore.

Todd, D. K. (1959), *Groundwater Hydrology*, Wiley, New York.

Wang, H. F. (2000), *Theory of Linear Poroelasticity*, Princeton Univ. Press, Princeton, N. J.

Watson, K. M., Y. Bock, and D. T. Sandwell (2002), Satellite interferometric observations of displacements associated with seasonal groundwater in the Los Angeles basin, *J. Geophys. Res.*, 107(B4), 2074, doi:10.1029/2001JB000470.

Whitcomb, J. H., J. D. Garmany, and D. L. Anderson (1973), Earthquake prediction: Variation of seismic velocities before the San Francisco earthquake, *Science*, 180, 632–635.

Zhan, Z., and R. W. Clayton (2010), Apparent velocity change caused by temporal variation of frequency content of ambient seismic noise, Abstract S21D-08 presented at 2010 Fall Meeting, AGU, San Francisco, Calif., 13–17 Dec.

V. C. Tsai, Geologic Hazards Science Center, U.S. Geological Survey, 1711 Illinois St., Golden, CO 80403, USA. (vtsai@post.harvard.edu)